Defining cell population diversity and T cell dysfunction in a mouse model of obesity

Using the BD FACSymphony™ A5 Cell Analyzer and BD Horizon™ Red 718 Reagent to empower the resolution of CD107a, a functional marker of cell degranulation

Features

- Streamlined workflow to obtain and characterize immune cells from fat, blood and spleen
- Combining cell based-assays with high–parameter flow cytometry for assessment of T cell function
- Showcasing the versatile use of the new BD Horizon™ Red 718 (R718) Fluorochrome for resolution of both surface and intracellular markers

Obesity creates a chronic inflammatory environment that can lead to an exhausted phenotype amongst T cells. As exhausted T cells lose their effector functions, obese patients may be at a higher risk to develop different disorders, including infectious diseases and cancer. Strikingly, obesity is associated with increased efficacy of PD-1 and PD-L1 blockade in both tumor-bearing mice and cancer patients. Exhausted T cells may express elevated levels of PD-1 and thus these patients may respond better to PD-1-blockade immunotherapy.

In this study, we present a stepwise approach for intracellular staining and assessment of various immune cell types in a mouse model of obesity using a 21-color broad immunophenotyping panel. We then employed a separate 12-color functional panel to provide insights into obesity-associated T cell dysfunction and its potential implications in cancer progression and treatment.

BD

The model consisted of C57BL/6 mice that were fed a high fat diet (HFD) for a period of 4 or 16 weeks. In doing so, we could address progressive changes caused by the HFD over time. In addition to epididymal fat tissue, which harbors local inflammation condition in obese mice, we examined immune cell populations in blood and spleen. This allowed a thorough characterization of tissue-specific immune cell phenotypes and their relationship with obesity (Figure 1A). In addition, we performed an in vitro functional assay for assessment of T cell proliferation and expression of activation markers to determine T cell function in obesity (Figure 1B).

Figure 1A

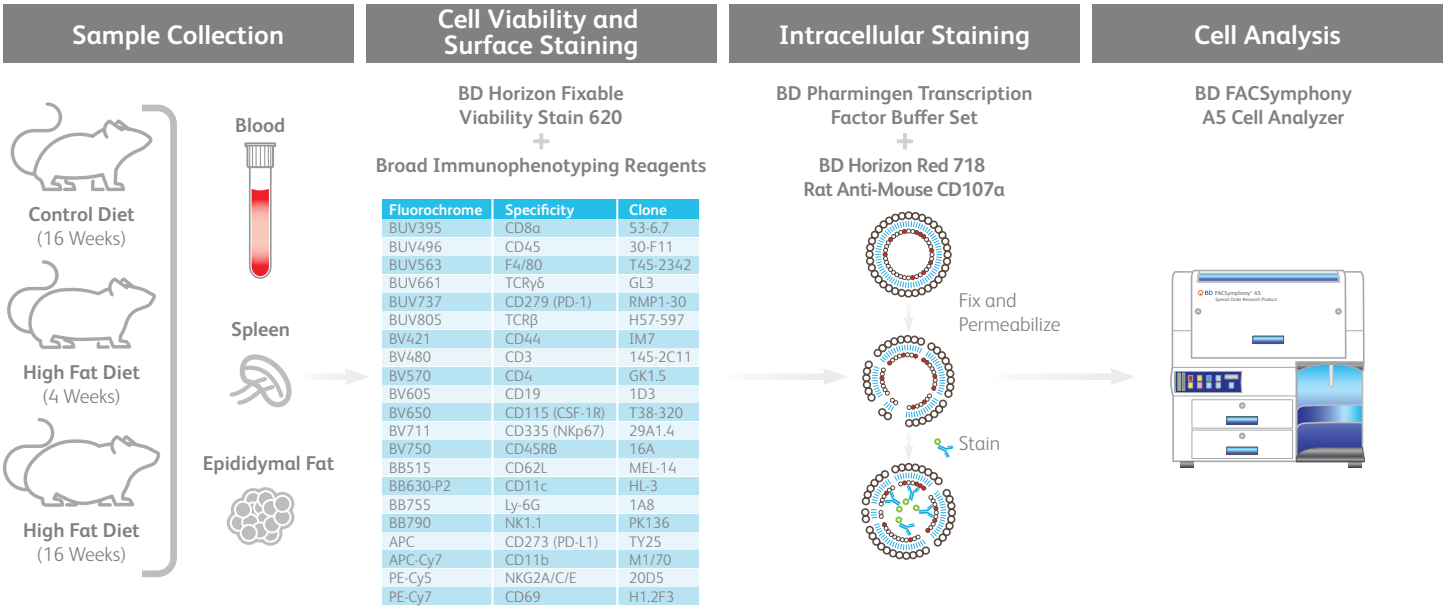

Fluorochrome	Specificity	Clone
BUV395	CD8a	53-6.7
BUV496	CD45	30-F11
BUV563	F4/80	T45-2342
BUV661	TCRγδ	GL3
BUV737	CD279 (PD-1)	RMP1-30
BUV805	TCRβ	H57-597
BV421	CD44	IM7
BV480	CD3	145-2C11
BV570	CD4	GK1.5
BV605	CD19	1D3
BV650	CD115 (CSF-1R)	T38-320
BV711	CD335 (NKp67)	29A1.4
BV750	CD45RB	16A
BB515	CD62L	MEL-14
BB630-P2	CD11c	HL-3
BB755	Ly-6G	1A8
BB790	NK1.1	PK136
APC	CD273 (PD-L1)	TY25
APC-Cy7	CD11b	M1/70
PE-Cy5	NKG2A/C/E	20D5
PE-Cy7	CD69	H1.2F3

Figure 1B

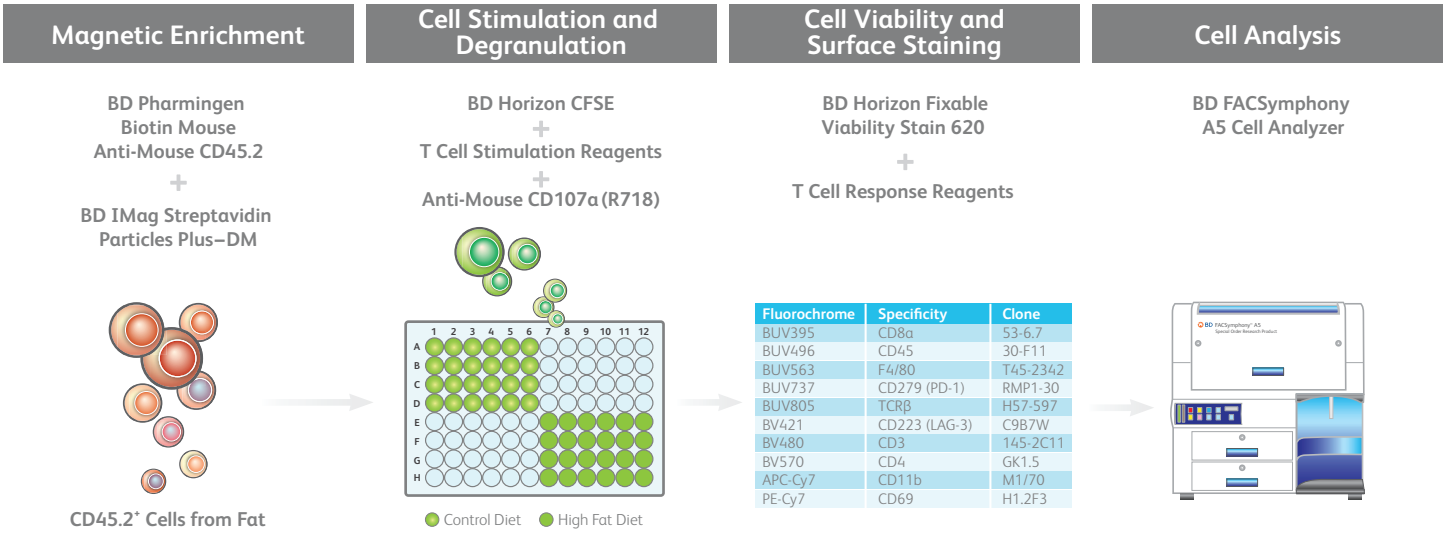

Fluorochrome	Specificity	Clone
BUV395	CD8a	53-6.7
BUV496	CD45	30-F11
BUV563	F4/80	T45-2342
BUV737	CD279 (PD-1)	RMP1-30
BUV805	TCRβ	H57-597
BV421	CD223 (LAG-3)	C9B7W
BV480	CD3	145-2C11
BV570	CD4	GK1.5
APC-Cy7	CD11b	M1/70
PE-Cy7	CD69	H1.2F3

Figure 1. Analysis of immune cell types across different tissues and assessment of T cell responses in a diet-induced obesity mouse model

A. Six-week-old C57BL/6 mice were placed on either a control diet or HFD for 4 or 16 weeks. Blood, spleens and epididymal fat were collected from two mice of each group. Spleen and fat tissues were both mechanically dissociated, and fat was further digested in a solution containing collagenase II (STEMCELL Technologies). The whole blood, spleen and fat tissue cells were treated with BD Pharm Lyse™ Lysing Buffer for red blood cell lysis. Splenocytes or fat tissue cells from the mouse duplicates were combined before staining to increase cell number. Single-cell suspensions were stained with a fixable viability dye (FVS620) to monitor cell viability. Cells were washed and stained with a cocktail of surface markers in the presence of Mouse BD Fc Block™ Reagent and BD Horizon Brilliant Stain Buffer Plus. Then, the cells were fixed and permeabilized using the BD Pharmingen Transcription Buffer Set and intracellularly stained with R718 anti-mouse CD107a. The cells were acquired using the BD FACSymphony A5 Cell Analyzer. **B.** Single-cell suspensions were prepared as described in Figure 1A and CD45.2$^+$ cells were purified from fat after staining with biotin anti-mouse CD45.2 and magnetic separation with streptavidin. The cells were labeled with carboxyfluorescein diacetate succinimidyl ester (CFSE) and cultured with immobilized BD Pharmingen Purified NA/LE Hamster Anti-Mouse CD3e and soluble BD Pharmingen Purified NA/LE Hamster Anti-Mouse CD28 for 3 days. During the final 5 hours of culture, the cells were incubated in the presence of R718 anti-mouse CD107a and T cell activation reagents consisting of phorbol myristate acetate (PMA), ionomycin, and BD GolgiPlug™ and BD GolgiStop™ Protein Transport Inhibitors. The cells were removed from the plates, stained with FVS620 and additional T cell response reagents, then analyzed on a BD FACSymphony A5 Cell Analyzer.

To delineate the main immune cell populations in blood, spleen and fat, we employed a broad 21-color immunophenotyping panel for detection of surface and intracellular targets (Figure 1A). The gating strategy shown in Figure 2A represents cells from a control-diet mouse and allowed a high-level cell analysis across tissues. All tissues had clearly distinguished natural killer (NK) cells, B cells and T cell subsets. In blood and spleen, three populations of CD11b$^+$ myeloid cells were detected based on the expression of CD11c and Ly-6G. The Ly-6G$^+$ cells correspond to primarily neutrophils, while Ly-6G$^-$ cells may include monocytes, macrophages and dendritic cells. In the fat, Ly-6G$^+$ cell frequency was lower than in blood and spleen and further characterization of the CD11b$^+$ population showed the presence of F4/80$^+$ macrophages in this tissue (Figure 2B).

CD107a or lysosome-associated membrane protein 1 (LAMP1) is ubiquitously expressed and resides primarily across lysosomal membranes. When measured intracellularly, CD107a expression levels can be used to determine the size of lysosomes/granules compartments and to assess various cellular processes such as phagocytosis, autophagy and aging. Additionally, cells with migratory properties and cytotoxic functions may externalize CD107a. In these conditions, CD107a expression on the cell surface can be used to attest the onset of cell degranulation.

Analysis of the intracellular levels of CD107a in different cell types showed that CD11b$^+$ myeloid cells in the fat expressed the highest levels of CD107a (Figures 2B and 2C). Similarly, CD11b$^+$CD11c$^-$ and CD11b$^+$CD11c$^+$ populations in the blood presented high and intermediate levels of CD107a while neutrophils and lymphocyte populations showed low levels (Figure 2C).

Figure 2A

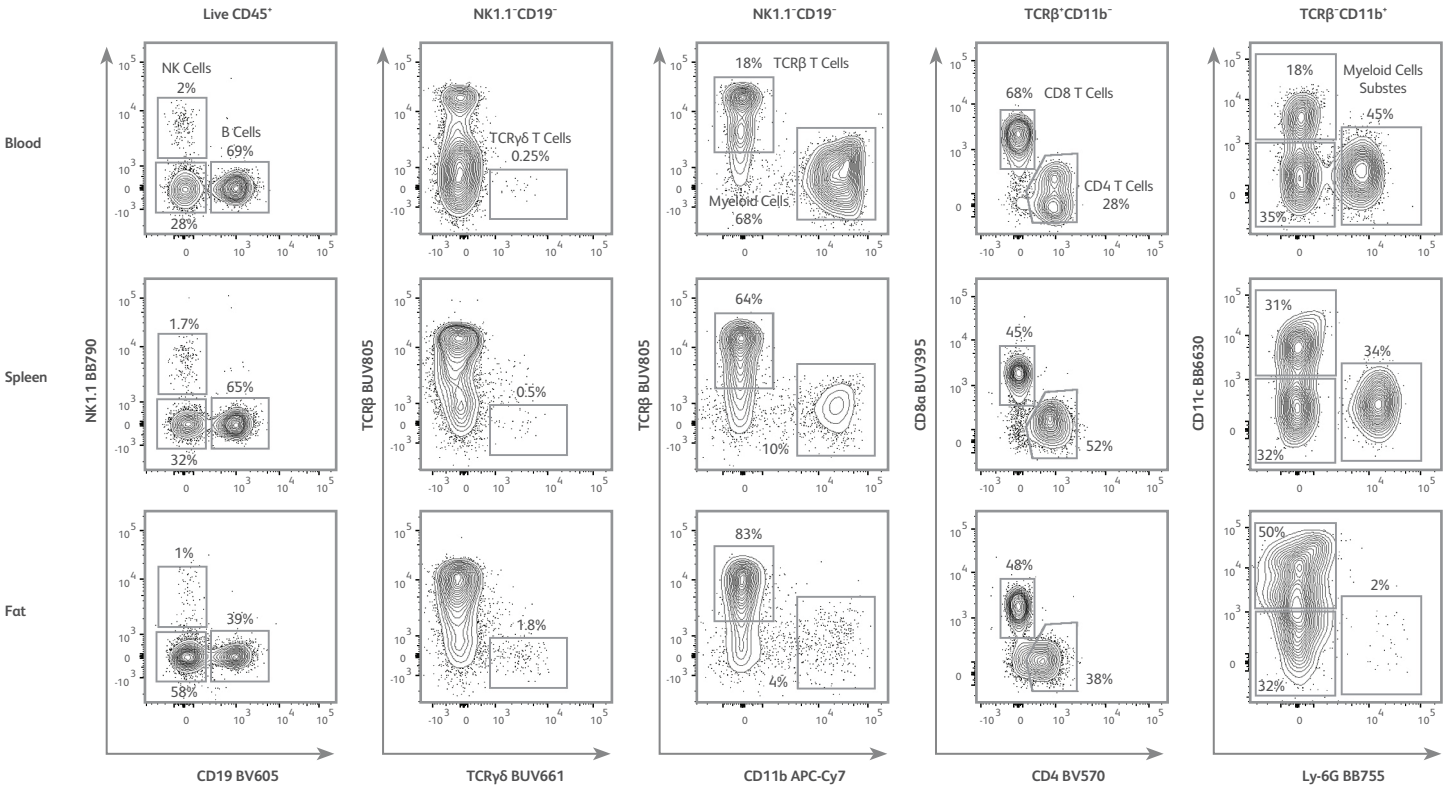

Figure 2B

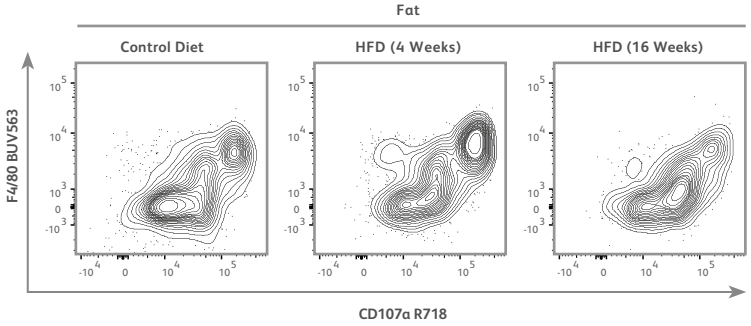

Figure 2C

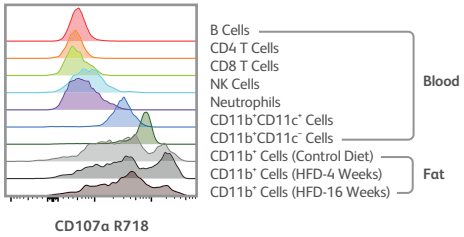

Figure 2. Classification of major immune cell types in different tissues

The cells were processed as described in Figure 1A. FVS620-positive cells and doublets were excluded before analysis of NK cells, B cells, T cell subsets and myeloid cells subsets among CD45$^+$ cells. **A.** Representative data showing the staining of tissues from mice fed with a control diet. **B.** Comparison between fat CD11b$^+$ myeloid cells from control diet, HFD (4 weeks) and HFD (16 weeks), showing a continuous CD107a expression from low to high levels in all mice. **C.** Histogram overlays showing CD107a expression in different cell types from blood or fat. The bottom three histograms show a higher CD107a expression in fat CD11b$^+$ cells compared to cell types in blood.

Further cell analyses and comparisons between mice were performed after dimensionality reduction of the data using the Uniform Manifold Approximation and Projection (UMAP) algorithm in FlowJo™ Software, v10.6.2. Thirty thousand live CD45$^+$ cells from each sample were concatenated and projected on the UMAP plot. To obtain a general classification of the clusters into B cell, T cell, NK cell and myeloid cell populations, the manually gated cells represented in Figure 2A were projected over ungated cells on the UMAP plot (Figure 3A). Next, cells from each tissue and mouse were separated and displayed individually on the UMAP for data visualization and comparisons (Figure 3B).

The following analyses focused on the T cell compartment to look for possible alterations in cell distribution. First, TCRγδ T cells were present mainly in the fat and were increased in HFD compared to control diet mice. Second, CD8 T cells showed a different clustering pattern as compared to the other tissues. The CD4 T cell clusters are also more heterogenous in spleen and fat compared to blood, however, there were no notable differences between HFD and control mice.

Figure 3A

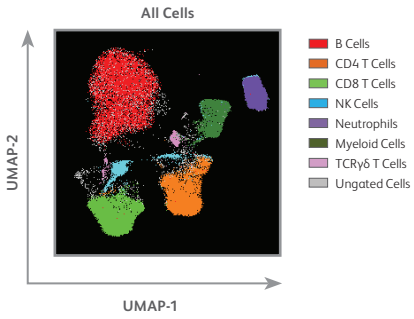

Figure 3B

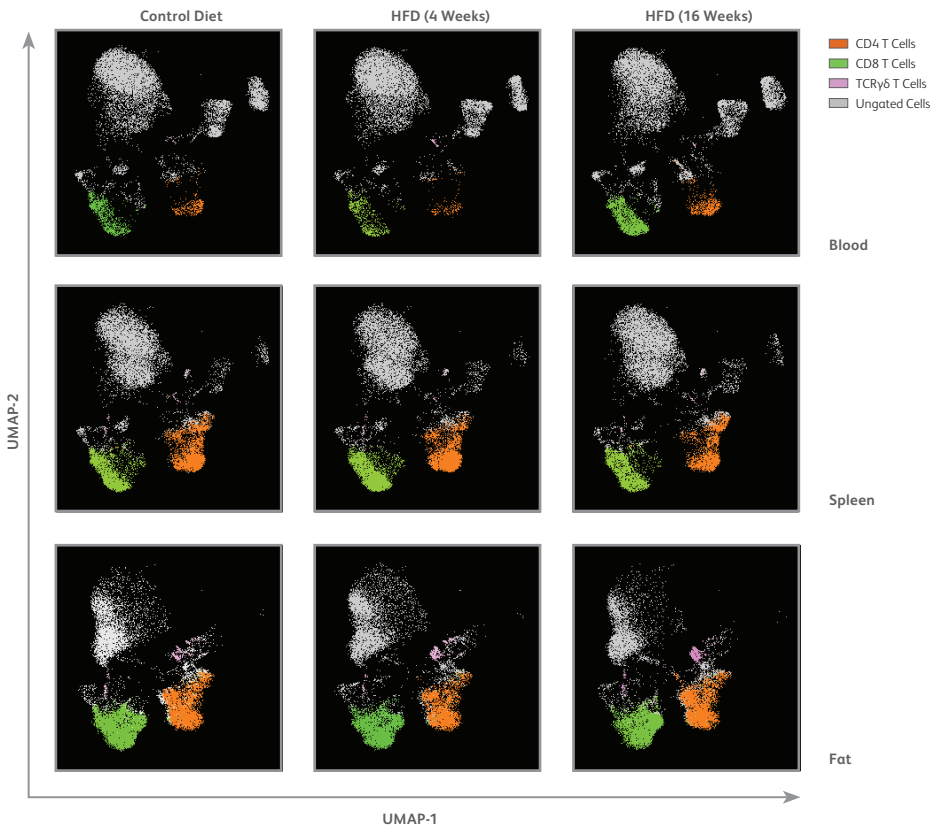

Figure 3. UMAP projection for visualization of cell populations across different tissues and mice

A. Thirty thousand live CD45$^+$ cells from each sample, a total of 270,000 cells, were used for generation of the UMAP. Cells manually gated in Figure 2A were displayed over the UMAP for identification of cell clusters. **B.** Overlays of gated CD4$^+$ T cells and CD8$^+$ T cells on the UMAP showed different clustering patterns in the fat compared to other tissues. The HFD (16 weeks) mice also had a larger cluster of TCRγδ T cells in fat compared to HFD (4 weeks) and control mice.

Application of the PhenoGraph algorithm (FlowJo Software) for an unbiased cell clustering approach confirmed the heterogeneity within the CD8 T cell population in the fat (Figure 4A). Phenograph clusters were designated as "PG-xx" with "xx" being the cluster number. Three major CD8 T cell clusters (PG-6, PG-11 and PG-26) were identified in the fat of all mice and also a fourth cluster (PG-15) that was increased in HFD (16 weeks) compared to HFD (4 weeks) and control diet mice (Figure 4B). Strikingly, PhenoGraph detected TCRγδ T cells as a unique cell cluster (PG-31). The identity of the PG-31 cluster as TCRγδ T cells was confirmed by overlaying this cluster on manually gated cells for analysis of TCRβ versus TCRγδ expression (Figure 4C). Likewise, the overlay of PG-15 over manually gated CD8 T cells revealed that this cluster contained effector and memory cells (CD62L$^-$CD44$^-$ or CD62L$^-$CD44$^+$ cells). The latter analysis also showed that the proportions of effector and memory cells were higher in HFD (16 weeks) compared to the other mice.

However, HFD and control mice presented similar proportions of T cell subsets in the spleen, indicating that the alteration observed in obese mice was limited to the fat tissue (Figure 4C).

Figure 4A

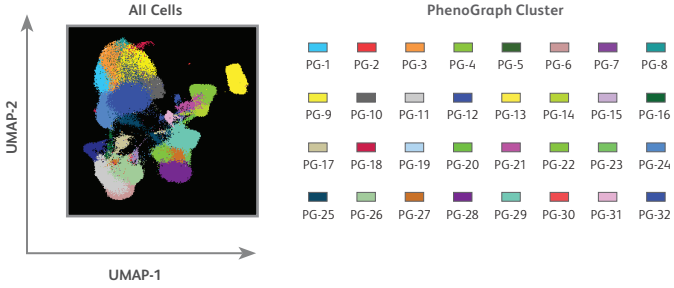

Figure 4B

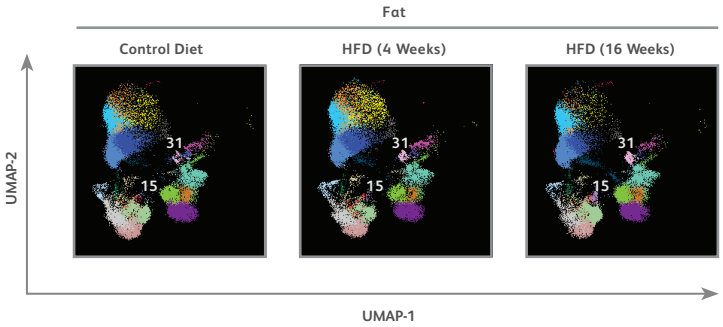

Figure 4C

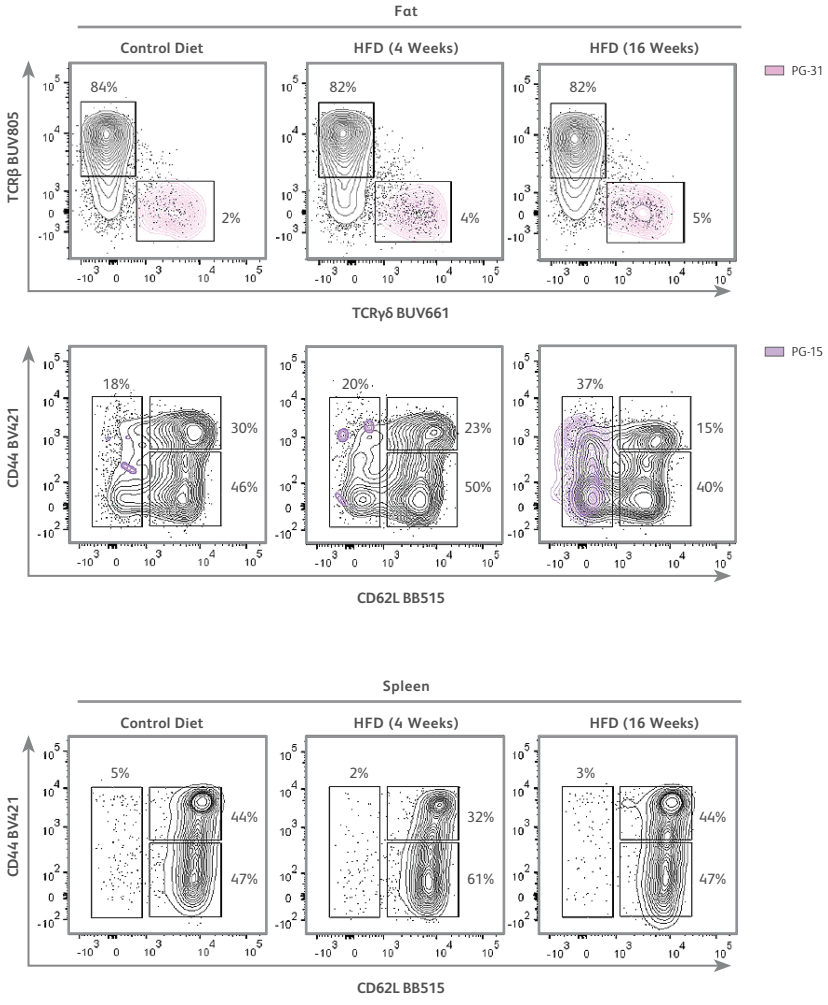

Figure 4. Unbiased identification of cell populations using the PhenoGraph algorithm

A. UMAP projection contains 30,000 cells from each sample and displays the overlays of PhenoGraph colored clusters. **B.** Analysis of PhenoGraph clusters in fat tissues of the different mice. PhenoGraph clusters 15 and 31 present higher numbers of cell events in HFD mice. **C.** Overlay of PG-31 on manually gated live CD45$^+$ cells confirm the identity of the cluster as TCRγδ T cells (top row) and the increased frequency in HFD (16 weeks) mice. PG-15 overlay on fat CD8$^+$ T cells shows these cells might correspond to CD62L$^-$ effector and memory cells (middle row). These latter populations are increased in the fat of HFD mice. Conversely, CD62L$^-$ cells are rare and have a similar profile in the spleens of HFD and control-diet mice (bottom row).

To further evaluate the functional state of T cells in the obese mice, CD45.2$^+$ cells were purified from epididymal fat, loaded with CFSE and cultured for 3 days in the presence of immobilized anti-CD3 and soluble anti-CD28, as described in detail in Figure 1B. Five hours before cell harvest, we added PMA, ionomycin, protein transport inhibitors and BD Horizon R718 anti-CD107a Reagent to the cultures. This enabled us to measure T cell proliferation by CFSE dilution, the expression of activation markers and to assess cell degranulation based on CD107a expression on the cell surface.

As noted from the analysis of forward and side scatter, the control-diet cells showed a robust increase in cell size after a period of three days in culture. Analysis of CFSE dilution profile demonstrated that most of the control CD8 T cells underwent at least three rounds of cell division (Figure 5A). These cells also showed sustained expression of CD69 and PD-1 throughout proliferation and externalized CD107a as a sign of activation-induced cell degranulation (Figure 5B). In contrast, the HFD (16 weeks) cells presented smaller cell size and increased cell debris in culture (Figure 5A). Although the remaining live CD8 T cells upregulated CD69, PD-1 and surface CD107a, these cells proliferated at a lower rate than control cells in response to stimulation (Figure 5B). Spleen CD8 T cells from HFD and control-diet mice survived and proliferated similarly (data not shown).

Figure 5A

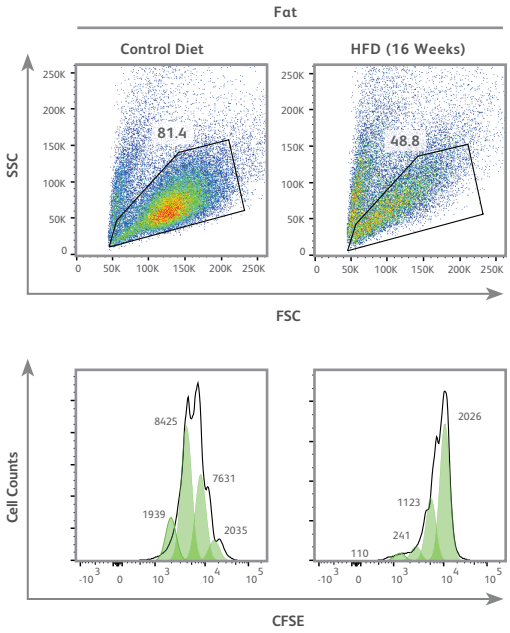

Figure 5B

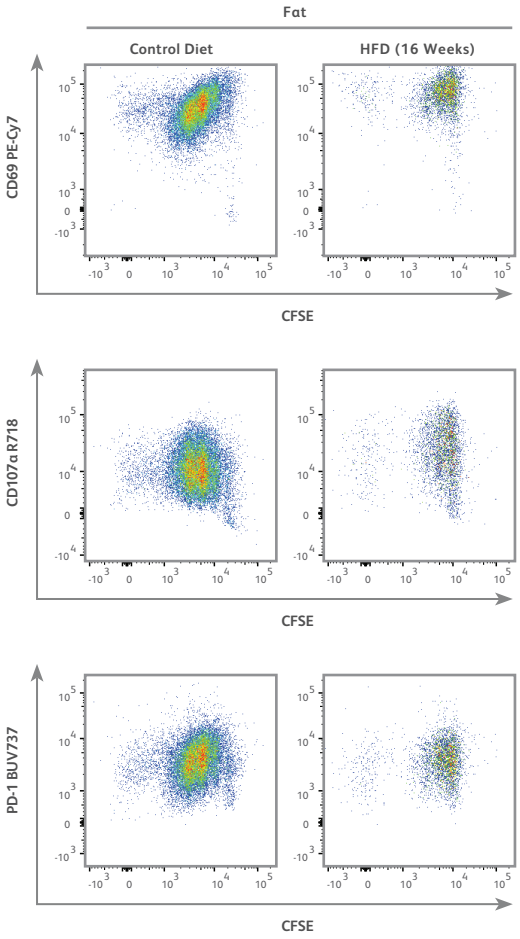

Figure 5. In vitro assessment of CD8 T cell function

CD45.2$^+$ cells were magnetically purified from fat tissue and cultured as described in Figure 1B. **A.** Evaluation of cell size using forward and side scatter characteristics (top) revealed lower frequency of cells in the live gate of the HFD compared with control-diet cultures. Analysis of CFSE dilution on gated CD45$^+$CD8$^+$ cells showed less cell division in the HFD culture. **B.** The remaining live CD45$^+$CD8$^+$ cells from the HFD mouse upregulated CD69, surface CD107a and PD-1 but proliferated less.

Reports in the literature have shown that dysfunctional or exhausted T cells can be found in the fat of obese mice. The proposed workflows revealed differences in cell composition across the different tissues. In this regard, intracellular measurement of CD107a corroborated to distinguish cell phenotypes, especially myeloid cell subsets. Notably, HFD caused an increase in the frequency of effector/memory CD8 T cells and TCRγδ T cells in the fat. However, fat CD8 T cells from HFD mice proliferated less in vitro. Herein the analysis of CD107a expression on cell surface combined with the analysis of activation (CD69) and inhibitory (PD-1) markers contributed to a thorough characterization of CD8 T function in obesity.

Ordering information

Reagents	
Description	Cat. No.
BD OptiBuild™ BUV805 Hamster Anti-Mouse TCR β Chain	748405
BD OptiBuild™ BUV737 Rat Anti-Mouse CD279 (PD-1)	749306
BD OptiBuild™ BUV661 Hamster Anti-Mouse γδ T-Cell Receptor	750410
BD OptiBuild™ BUV563 Rat Anti-Mouse F4/80	749284
BD OptiBuild™ BUV496 Rat Anti-Mouse CD45	749889
BD Horizon™ BUV395 Rat Anti-Mouse CD8a	563786
BD OptiBuild™ BV750 Rat Anti-Mouse CD45RB	747252
BD OptiBuild™ BV711 Rat Anti-Mouse CD335 (NKp46)	740822
BD Horizon™ BV605 Rat Anti-Mouse CD19	563148
BD OptiBuild™ BV650 Rat Anti-Mouse CD115 (CSF-1R)	743641
BD OptiBuild™ BV480 Hamster Anti-Mouse CD3	746368
BD Horizon™ BV421 Rat Anti-Mouse CD44	563970
BD Horizon™ BB515 Rat Anti-Mouse CD62L	565261
BD Pharmingen™ PE-Cy7 Hamster Anti-Mouse CD69	552879

Custom Reagents	
Description	Cat. No.
BV570 Rat Anti-Mouse CD4	Custom
BB790 Mouse Anti-Mouse NK1.1	Custom
BB755 Rat Anti-Moue Ly-6G	Custom
BB630-P2 Hamster Anti-Mouse CD11c	Custom
PE-Cy5 Rat Anti-Mouse NKG2A/C/E	Custom

*These products are not available for general sale and were obtained for this experiment through our own custom conjugation service. BD offers special order and custom configuration products which are manufactured at the instruction and to specifications as provided by the buyer. Reach out to your sales representative for more details.

Reagents	
Description	Cat. No.
BD Pharmingen™ APC-Cy7 Rat Anti-CD11b	557657
BD OptiBuild™ BV421 Rat Anti-Mouse CD223	740072
BD Horizon™ Red 718 Anti-Mouse CD107a	566986
BD Horizon™ Fixable Viability Stain 620	564996
BD Pharmingen™ Transcription Factor Buffer Set	562725
BD Pharmingen™ Biotin Mouse Anti-Mouse CD45.2	553771
BD IMag™ Streptavidin Particles Plus - DM	557812
BD Horizon™ CFSE	565082
BD Pharmingen™ Purified NA/LE Hamster Anti-Mouse CD28	553294
BD Pharmingen™ Purified NA/LE Hamster Anti-Mouse CD3e	553057
BD GolgiStop™ Protein Transport Inhibitor (Containing Monensin)	554724
BD GolgiPlug™ Protein Transport Inhibitor (Containing Brefeldin A)	555029
BD Pharm Lyse™ Lysing Buffer	555899
BD Pharmingen™ Purified Rat Anti-Mouse CD16/CD32 (Mouse BD Fc Block™)	553141
BD Horizon™ Brilliant Stain Buffer Plus	566385

BD Flow Cytometers are Class 1 Laser Products.

For Research Use Only. Not for use in diagnostic or therapeutic procedures.

23-23574-00

BD Life Sciences, San Jose, CA, 95131, USA

bdbiosciences.com